AIP | Applied Physics Letters

Compact and broadband directional coupling and demultiplexing in dielectric-loaded surface plasmon polariton waveguides based on the multimode interference effect

Zhihong Zhu, Cesar E. Garcia-Ortiz, Zhanghua Han, Ilya P. Radko, and Sergey I. Bozhevolnyi

Citation: Appl. Phys. Lett. **103**, 061108 (2013); doi: 10.1063/1.4817860
View online: http://dx.doi.org/10.1063/1.4817860
View Table of Contents: http://apl.aip.org/resource/1/APPLAB/v103/i6
Published by the AIP Publishing LLC.

Compact and broadband directional coupling and demultiplexing in dielectric-loaded surface plasmon polariton waveguides based on the multimode interference effect

Zhihong Zhu,[1,2] Cesar E. Garcia-Ortiz,[1,3] Zhanghua Han,[1,a)] Ilya P. Radko,[1] and Sergey I. Bozhevolnyi[1,b)]
[1]*Institute of Technology and Innovation (ITI), University of Southern Denmark, Niels Bohrs Allé 1, DK-5230 Odense M, Denmark*
[2]*College of Optoelectronic Science and Engineering, National University of Defense Technology, Changsha 410073, People's Republic of China*
[3]*UANL, Facultad de Ciencias Físico-Matemáticas, San Nicolás de los Garza (NL) 66450, Mexico*

(Received 14 March 2013; accepted 24 July 2013; published online 6 August 2013)

We theoretically, numerically, and experimentally demonstrate that a directional coupling function can be realized with a wide bandwidth (greater than 200 nm) in dielectric-loaded surface plasmon polariton waveguides based on the multimode interference effect. The functional size of the structures is in the range of several micrometers, which is much shorter than traditional directional couplers consisting of two parallel dielectric or plasmonic metallic waveguides. In addition, 1×2 beam splitting and demultiplexing function was realized. Such devices with wide bandwidth and small size indicate potential applications in high density lab-on-chip photonic integration and circuits. © *2013 AIP Publishing LLC*. [http://dx.doi.org/10.1063/1.4817860]

Surface-plasmon polaritons (SPPs) open an opportunity for realizing chip-scale photonic integration circuits because of their ability to confine the electromagnetic wave below the diffraction limit.[1] In recent years, several kinds of SPP waveguide-based structures, such as long range surface plasmon waveguides, dielectric-loaded waveguides (DLSPPWs), metallic nanowires, and metal-insulator-metal waveguides, have been proposed.[1–7] Among these, DLSPPWs show a special advantage for high-density integration because of the relatively low bend and propagation loss, which facilitates large-scale industrial fabrication achievable with the existing lithography techniques. Therefore, many researchers seek photonic fundamental components using DLSPPW,[8–15] including beam splitters,[9,10] directional couplers,[11,15] Mach-Zehnder interferometers,[12–14] and ring resonators.[16,17] In addition, several multi-mode interference (MMI) structures based on DLSPPWs[18,19] combined with the thermo-optic effect have been demonstrated to realize optical switching controlled by electronic signals.[20–23] However, these studies paid little attention to the bandwidth of operation and the device length, which are keys for static high-speed signal operation.

In this work, we present a compact and broadband DLSPPW directional coupler based on the MMI effect. The proposed structures are analyzed theoretically and numerically in order to complement the experimental characterization which demonstrates these functions in the optical regime.

We start from studying a model system of a dielectric-loaded MMI structure, which consists of a polymethylmethacrylate (PMMA) layer with predefined three single-mode waveguides and one multimode region on the top of a gold film, which is supported by a thin glass substrate (Fig. 1(a)). The single-mode waveguides work as input and output waveguides (A and B, respectively), while the multimode waveguide serves as the MMI region. The geometrical parameters of the structure are as follows: the Au film thickness d is 50 nm; the PMMA layer thickness t is 300 nm; the PMMA width of the input waveguide is 290 nm; the PMMA width w of the multimode region is 740 nm; the radius of curvature of both output waveguides is 2000 nm (Fig. 1(a)). The Au is treated as a dispersive medium following the Drude model. The metal permittivity is derived by using $\varepsilon(\omega) = \varepsilon_\infty - \omega_p^2/(\omega^2 + i\omega/\tau)$, where ε_∞ is the interband-transition contribution to the permittivity, ω_p the bulk plasma frequency, and τ the mean free time between electron collisions. The values of ε_∞, ω_p, and τ are 1.0, 1.38×10^{16} rad/s, and 33 fs, respectively, obtained by fitting the experimental data Au from the literature.[24] The refractive indexes of PMMA and SiO_2 substrate are 1.484 and 1.50, respectively. Using a rigorous finite element method (FEM) implemented in a commercial software of COMSOL Multiphysics, the propagation constants of all the supported modes in the multimode region of the structure are calculated and plotted in Figs. 1(b) and 1(c) as a function of the wavelength. We can observe that the two guided modes (the fundamental DLSPPW mode and the first order mode) are supported in the multimode region. We also find two key points: one is that the difference between the imaginary part of the propagation constant of the two guided modes is approximately equal to 0 in a wide wavelength range of 620–900 nm, implying that the two modes have almost the same level of decaying and then the variation of the mode power is mainly determined by the interference between the modes. The second is that the difference between the real parts of their propagation constant is relatively large and varies slightly with the wavelength in the same wavelength range, and then the MMI effect can be observed in a relatively short distance.

a)Electronic mail: zhh@iti.sdu.dk
b)Electronic mail: seib@iti.sdu.dk

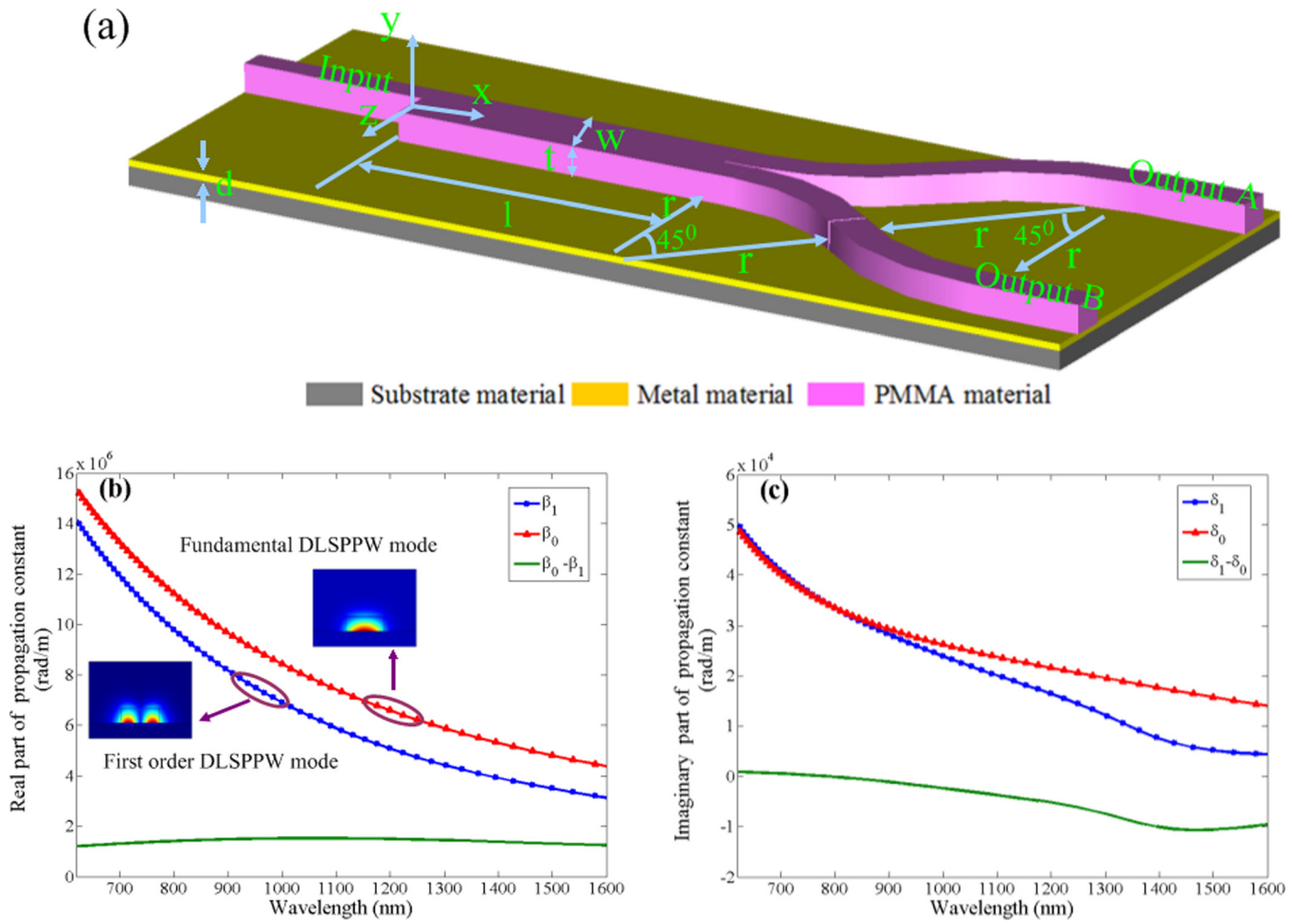

FIG. 1. (a) Schematic diagram of directional coupler consisting of a PMMA layer with predefined three single-mode waveguides and one multimode region on the top of a gold film. (b) Real part of propagation constant for all supported modes in the multimode region of the structure as a function of the wavelength. The inset shows the electric field patterns of the fundamental DLSPPW mode and the first order mode. (c) Imaginary part of the propagation constant of all the supported modes in the multimode region of the structure as a function of the wavelength.

Suppose we launch an input signal propagating along the x axis with a wavelength in the range of 620–900 nm into the input waveguide and two guided modes in the multimode region are excited. The total field $\vec{\psi}(x,y,z)$ in the multimode region can be expressed as a superposition of the two excited guided modes as

$$\vec{\psi}(x,y,z) = c_0\vec{\psi}_0(y,z)e^{-\delta_0 x}e^{-j\beta_0 x} + c_1\vec{\psi}_1(y,z)e^{-\delta_1 x}e^{-j\beta_1 x}, \tag{1}$$

where c_0, $\vec{\psi}_0$, δ_0, and β_0 denote the excitation coefficient, modal field distribution, and imaginary and real parts of the propagation constant of the fundamental DLSPPW mode, respectively. Similarly, c_1, $\vec{\psi}_1$, δ_1, and β_1 indicate the corresponding arguments of the first order mode. Because the imaginary parts of the propagation constants of the two modes are designed to be approximately equal in the range of 620–900 nm (Fig. 1(c)), we let δ replace δ_0 and δ_1. As the two output waveguides are placed at the back-end ($x = l$) of the multimode region, the output energy from the two output waveguides is directly determined by the modal field distribution $\vec{\psi}(l,y,z)$. For simplicity, the initial phase of the input field at $x = 0$ is assumed to be 0, and therefore the input field at $x = 0$ should be

$$\vec{\psi}(0,y,z) = c_0\vec{\psi}_0(y,z) + c_1\vec{\psi}_1(y,z). \tag{2}$$

If the phase difference $(\beta_0–\beta_1)l$ between the two interfering modes is equal to $2n\pi$ ($n = 1,2,3,\ldots$), the total field profile at the back-end of the multimode region can be written as

$$\vec{\psi}(l,y,z) = e^{-\delta l - j\beta_0 l}\vec{\psi}(0,y,z), \tag{3}$$

indicating that the power from the input signal is only transferred to the output waveguide A. However, if the phase difference between the two interfering modes is equal to $(2n+1)\pi$ ($n = 1,2,3,\ldots$), the total field profile at the end of the multimode region can be written as

$$\vec{\psi}(l,y,z) = e^{-\delta l - j\beta_0 l}[c_0\vec{\psi}_0(y,z) - c_1\vec{\psi}_1(y,z)]. \tag{4}$$

Considering the even and odd symmetry of two excited guided modes, the field can be expressed as

$$\vec{\psi}(l,y,z) = e^{-\delta l - j\beta_0 l}\vec{\psi}(0,y,-z), \tag{5}$$

implying that the structure only transfers power from the input waveguide to the output B. Therefore, the directional coupling in dielectric-loaded plasmonic waveguides based

on the MMI effect is realized. Since $(\beta_0–\beta_1)$ is relatively large (greater than 1.0×10^6 rad/m) and varies slightly in the wavelength range of 620–900 nm, we can expect broadband directional coupling operation in a compact region (in the range of several micrometers).

To verify the theoretical prediction, we next performed numerical simulations using the finite-difference time-domain method.[25,26] Figs. 2(a) and 2(b) show the transmission from outputs A and B as a function of the input signal wavelength and the multimode region length. The corresponding transmission spectra when l equals to 2100 nm, 4200 nm, and 6000 nm are also shown in Figs. 2(c)–2(e), respectively. Fig. 2(c) shows that for $l = 2100$ nm at a wavelength of 730 nm, ~54% of the power from the input waveguide is transferred to the output waveguide B while only ~0.4% of the power transmits to the output waveguide A. Comparatively, at the same wavelength, about 44% of the power is transferred to the output waveguide A, and only ~1% of the power transmits from output waveguide B when $l = 4200$ nm. From Figs. 2(c) and 2(d), we can also see that the directional coupling operation can be achieved in a wide wavelength range of 650–850 nm with an isolation ratio greater than 10 dB. These results clearly show that the wideband directional coupling function can be realized by multimode DLSPPWs with a length of only several micrometers. The directional coupling operation can also be obtained when $l = 6300$ nm or 8400 nm, which correspond to the phase difference $(\beta_0–\beta_1)l$ between the two interfering modes to be 3π and 4π, respectively (Figs. 2(a) and 2(b)). Since the output power from the two output waveguides in the dielectric-loaded MMI structure is a function of l and the input signal wavelength, the wavelength-selective splitting function can be achieved when l is fixed. From Fig. 2(e), we can see that the transmission at 620 nm from output A is about 26% when $l = 6000$ nm, while the transmission from output B is about 5%. Comparatively, for the wavelength of 866 nm, the transmission from output A and B are around 2.3% and 32%, respectively. These simulation results clearly depict that for wavelengths of 620 nm and 866 nm the demultiplexing function is achieved. In addition, we also find that a 1×2 beam splitting function is directly obtained at 690 nm in the same structure.

In general, finite difference time domain (FDTD) simulations are difficult to conduct so as to precisely take into account experimental conditions because of need for the accurate representation of dispersion of the materials involved (especially metals). In addition, dimension mismatch might occur between the designed and fabricated structures. For these reasons, the above simulations should only be considered as guidelines for the experiments described below. Experimental samples were fabricated by sputtering Au onto a quartz substrate and afterwards spin-coated with a PMMA layer. The waveguide structures were fabricated by electron beam lithography. Figure 3(a) shows an optical microscopy image of a typical structure fabricated in this work. The performance of the fabricated components was characterized using leakage radiation microscopy (LRM). All input waveguides are connected to funnel structures which facilitate efficient excitation of the DLSPPW modes. The DLSPP modes are excited by illuminating the taper of the structure at normal incidence with a moderately focused beam (~5 μm) of a Ti:Sapphire laser. An oil-immersion objective with high

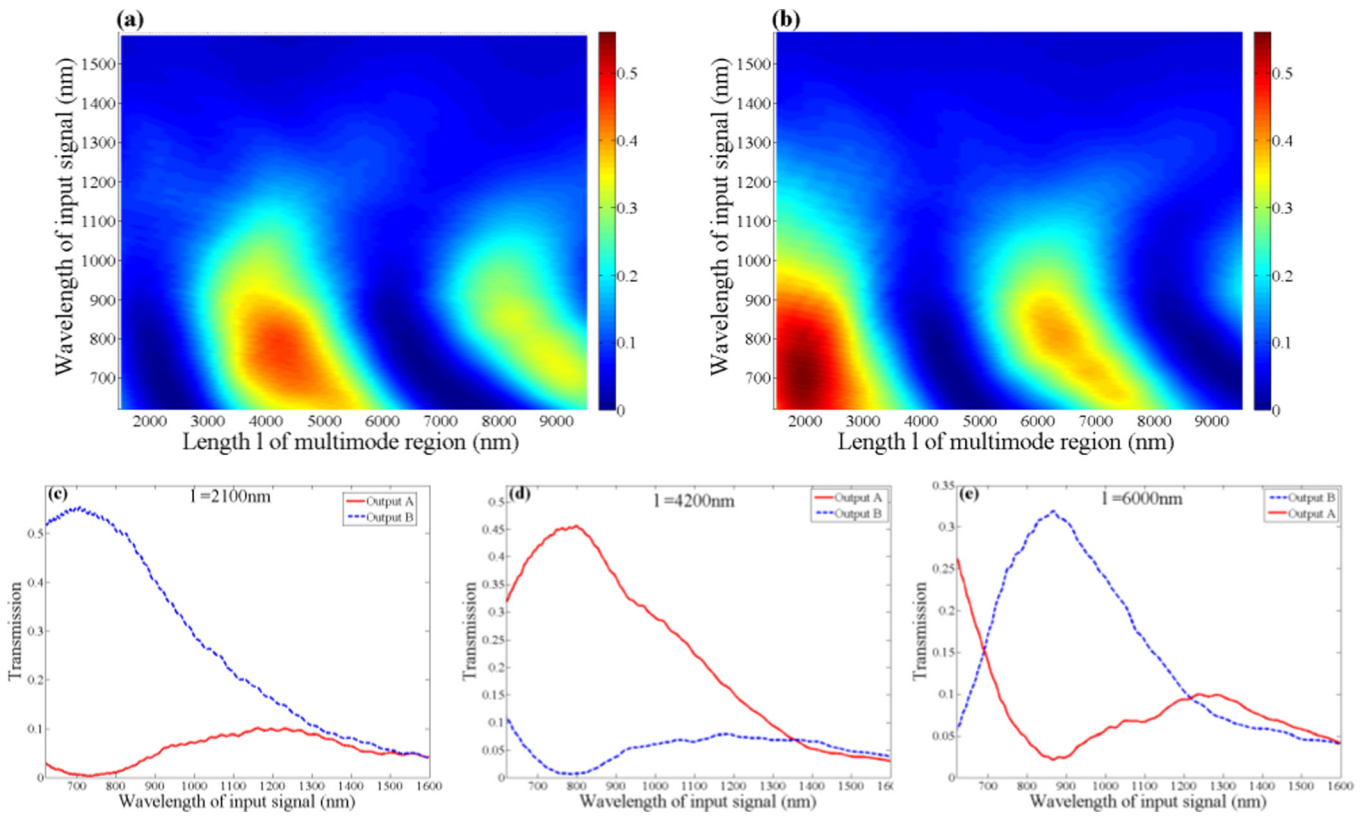

FIG. 2. Transmission from output (a) A and (b) B as a function of the input signal wavelength and the multimode region length. Different colors correspond to different values of the transmission. Transmission as a function of wavelength for (c) $l = 2100$ nm, (d) $l = 4200$ nm, and (e) $l = 6000$ nm.

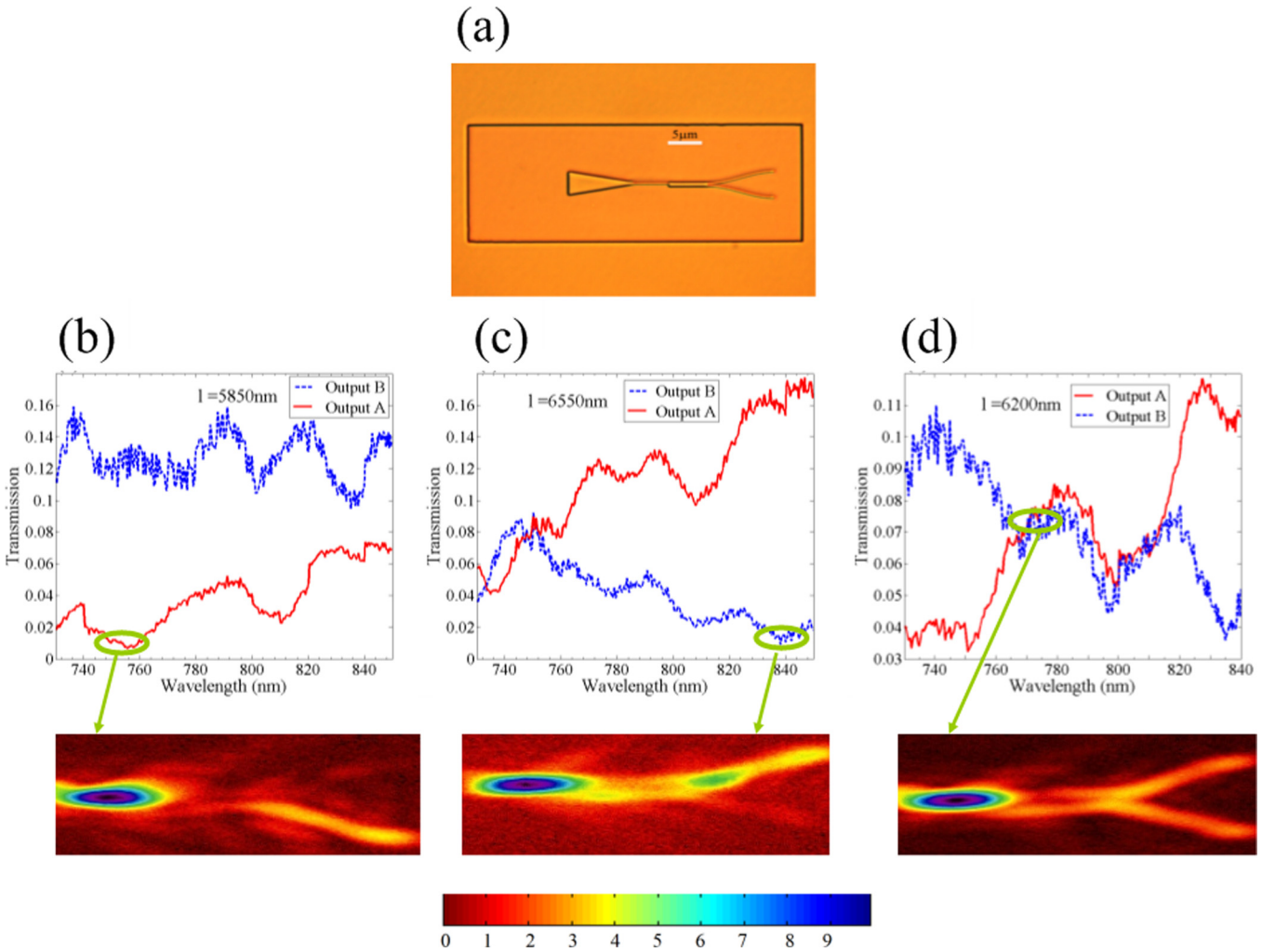

FIG. 3. (a) Optical microscopy of a typical fabricated structure. (b) Experimentally measured transmission spectra for $l = 5850$ nm, and LRM image at the wavelength of 756 nm. (c) Experimentally measured transmission spectra for $l = 6550$ nm, and LRM image at the wavelength of 838 nm. (e) Experimentally measured transmission spectra for $l = 6200$ nm, and LRM image at the wavelength of 765 nm.

numerical aperture NA = 1.45 that was used for collecting the leakage radiation was imaged using a CCD camera. The transmission was measured by analyzing the averaged intensity profiles of every LRM image at a point close to the input where the maximum value is found (point A) and a fixed point at the near the output (point B). Transmission is then calculated dividing the intensity values obtained at points A and B. This procedure is repeated for every LRM image taken at different wavelengths. The measured transmission spectra from output A and B for $l = 5850$ nm, 6550 nm, and 6200 nm are shown in Figs. 3(b)–3(d), respectively. The included LRM images clearly show and confirm the expected operative function. From Figs. 3(b) and 3(c), one can observe that most of the power of the input waveguide is transferred to output B when $l = 5850$ nm in the wavelength range of 760–850 nm. However, in the same wavelength range, most of the power is transferred to output A when $l = 6550$ nm. These experimental results further confirm that the compact and broadband directional coupling function can be achieved experimentally with multimode DLSPPWs. In Fig. 3(d), the transmission at 738 nm from the output A is about 4%, while the transmission from the output B is about 10%. Comparatively, the transmission at 838 nm from the outputs A and B are around 11% and 4%, respectively. Such results imply that the demultiplexing function is realized experimentally with the multimode DLSPPW with length in the range of several micrometers. In addition, Fig. 3(d) shows that a 1×2 beam splitting function can be directly obtained at 765 nm in the same structure. Comparing simulations (Fig. 2) and measurements (Fig. 3), we conclude that the predicted compact and broadband directional coupling in dielectric-loaded plasmonic waveguides based on the multimode interference effect is possible. However, the operation wavelength and transmission in simulations and measurements deviate from each other if the same parameters are used. This is due to the fact that the width and thickness of the PMMA ridge is in the range of several hundreds of nanometers and is difficult to be controlled accurately under our experimental environment, which results in different values of width and thickness compared to the original designed values. So, in this paper, we seek the agreement of physical phenomenon between experiment and simulation and do not importune a very strictly corresponding relation between them.

In summary, both simulation and experimental phenomena clearly show that the broadband directional coupling and demultiplexing function can be achieved with multimode

DLSPPW relatively small structures (in the range of several micrometers). The fact that the device is much shorter than traditional directional couplers consisting of two parallel dielectric or plasmonic metallic waveguides results from two points: one is because the interference effect is much stronger than the evanescent wave coupling between parallel waveguides. The second is that the propagation constant difference between fundamental DLSPPW mode and the first order mode is relatively large. The wide bandwidth of the device is due to the fact that the propagation constant differences between the two operation modes vary slightly with the wavelength of the light.

This work was supported by the Danish Council for Independent Research (the FTP project ANAP, Contract No. 09-072949), the State Key Program for Basic Research of China (No. 2012CB933501), and the National Natural Science Foundation of China (Grant Nos. 61177051, 61107042, and 61205087). C. E. Garcia-Ortiz would like to acknowledge the support from Facultad de Ciencias Fisico-Matematicas and scholarship from CONACYT (No. 228959).

[1]W. L. Barnes, A. Dereux, and T. W. Ebbesen, Nature (London) **424**, 824–830 (2003).
[2]L. Y. M. Tobing, L. Tjahjana, and D. H. Zhang, Appl. Phys. Lett. **101**, 041117 (2012).
[3]D. Rossouw and G. A. Botton, Phys. Rev. Lett. **110**, 066801 (2013).
[4]A. V. Krasavin and A. V. Zayats, Appl. Phys. Lett. **97**, 041107 (2010).
[5]S. Massenot, J. Grandidier, A. Bouhelier, G. C. des Francs, L. Markey, J. C. Weeber, A. Dereux, J. Renger, M. U. Gonz'alez, and R. Quidant, Appl. Phys. Lett. **91**, 243102 (2007).
[6]Y. Peng and K. Kempa, Appl. Phys. Lett. **100**, 171903 (2012).
[7]Y.-J. Tsai, A. Degiron, N. M. Jokerst, and D. R. Smith, Opt. Express **17**, 17471–17482 (2009).
[8]A. V. Krasavin and A. V. Zayats, Appl. Phys. Lett. **90**(21), 211101 (2007).
[9]X. Gao, J. H. Shi, X. P. Shen, H. F. Ma, W. X. Jiang, L. M. Li, and T. J. Cui, Appl. Phys. Lett. **102**, 151912 (2013).
[10]G. Yuan, P. Wang, Y. Lu, and H. Ming, Opt. Express **17**, 12594–12600 (2009).
[11]B. Steinberger, A. Hohenau, H. Ditlbacher, F. R. Aussenegg, A. Leitner, and J. R. Krenn, Appl. Phys. Lett. **91**(8), 081111 (2007).
[12]T. Holmgaard, S. I. Bozhevolnyi, L. Markey, and A. Dereux, Appl. Phys. Lett. **92**(1), 011124 (2008).
[13]T. Holmgaard, S. I. Bozhevolnyi, L. Markey, A. Dereux, A. V. Krasavin, P. Bolger, and A. V. Zayats, Phys. Rev. B **78**(16), 165431 (2008).
[14]A. V. Krasavin and A. V. Zayats, Phys. Rev. B **78**(4), 045425 (2008).
[15]Z. Chen, T. Holmgaard, S. I. Bozhevolnyi, A. V. Krasavin, A. V. Zayats, L. Markey, and A. Dereux, Opt. Lett. **34**(3), 310–312 (2009).
[16]Z. Han, C. E. Garcia-Ortiz, I. P. Radko, and S. I. Bozhevolnyi, Opt. Lett. **38**(6), 875–877 (2013).
[17]J. Gosciniak, S. I. Bozhevolnyi, T. B. Andersen, V. S. Volkov, J. Kjelstrup-Hansen, L. Markey, and A. Dereux, Opt. Express **18**(2), 1207–1216 (2010).
[18]C. Reinhardt, A. Seidel, A. B. Evlyukhin, W. Cheng, and B. N. Chichkov, J. Opt. Soc. Am. B **26**(12), B55–60 (2009).
[19]C. Reinhardt, A. Seidel, A. B. Evlyukhin, W. Cheng, R. Kiyan, and B. N. Chichkov, Appl. Phys. A **100**(2), 347–352 (2010).
[20]D. Kalavrouziotis, S. Papaioannou, K. Vyrsokinos, L. Markey, A. Dereux, G. Giannoulis, D. Apostolopoulos, H. Avramopoulos, and N. Pleros, IEEE Photonics Technol. Lett. **24**(20), 1819–1822 (2012).
[21]A. Pitilakis and E. E. Kriezis, J. Lightwave Technol. **29**(17), 2636–2646 (2011).
[22]K. Hassan, J. C. Weeber, L. Markey, A. Dereux, A. Pitilakis, O. Tsilipakos, and E. E. Kriezis, Appl. Phys. Lett. **99**, 241110 (2011).
[23]J. C. Weeber, K. Hassan, A. Bouhelier, G. Colas-des-Francs, J. Arocas, L. Markey, and A. Dereux, Appl. Phys. Lett. **99**, 031113 (2011).
[24]P. B. Johnson and R. W. Christy, Phys. Rev. B **6**, 4370 (1972).
[25]A. Taflove and S. C. Hagness, *Computational Electrodynamics: The Finite-Difference Time-Domain Method* (Artech House, 2000).
[26]Z. H. Zhu, W. M. Ye, J. R. Ji, X. D. Yuan, and C. Zen, Appl. Phys. B **86**(2), 327–331 (2007).